Acta Crystallographica Section D
Biological Crystallography
ISSN 0907-4449

The three-dimensional structure of MAP kinase p38β: different features of the ATP-binding site in p38β compared with p38α

Sangita B. Patel,[a] Patricia M. Cameron,[b] Stephen J. O'Keefe,[b] Betsy Frantz-Wattley,[c] Jed Thompson,[c] Edward A. O'Neill,[c] Trevor Tennis,[d] Luping Liu,[d] Joseph W. Becker[a] and Giovanna Scapin[a]*

[a]Department of Global Structural Biology, Merck Research Laboratory, PO Box 2000, Rahway, NJ 07065, USA, [b]Department of Immunology, Merck Research Laboratory, PO Box 2000, Rahway, NJ 07065, USA, [c]Department of Cardiovascular Diseases, Merck Research Laboratory, PO Box 2000, Rahway, NJ 07065, USA, and [d]Department of Medicinal Chemistry, Merck Research Laboratory, PO Box 2000, Rahway, NJ 07065, USA

Correspondence e-mail: giovanna.scapin@spcorp.com

Received 21 February 2009
Accepted 28 April 2009

PDB References: MAP kinase p38α, inhibitor complex, 3gc7, r3gc7sf; MAP kinase p38β, C162S mutant, 3gc8, r3gc8sf; C119S,C162S mutant, 3gc9, r3gc9sf.

The p38 mitogen-activated protein kinases are activated in response to environmental stress and cytokines and play a significant role in transcriptional regulation and inflammatory responses. Of the four p38 isoforms known to date, two (p38α and p38β) have been identified as targets for cytokine-suppressive anti-inflammatory drugs. Recently, it was reported that specific inhibition of the p38α isoform is necessary and sufficient for anti-inflammatory efficacy *in vivo*, while further inhibition of p38β may not provide any additional benefit. In order to aid the development of p38α-selective compounds, the three-dimensional structure of p38β was determined. To do so, the C162S and C119S,C162S mutants of human MAP kinase p38β were cloned, expressed in *Escherichia coli* and purified. Initial screening hits in crystallization trials in the presence of an inhibitor led upon optimization to crystals that diffracted to 2.05 Å resolution and allowed structure determination (PDB codes 3gc8 and 3gc9 for the single and double mutant, respectively). The structure of the p38α C162S mutant in complex with the same inhibitor is also reported (PDB code 3gc7). A comparison between the structures of the two kinases showed that they are highly similar overall but that there are differences in the relative orientation of the N- and C-terminal domains that causes a reduction in the size of the ATP-binding pocket in p38β. This difference in size between the two pockets could be exploited in order to achieve selectivity.

1. Introduction

The p38 family of mitogen-activated protein kinases are activated in response to environmental stress and cytokines. Four isoforms of p38 kinases have been identified so far: p38α (also known as RK, p38, EXIP, Mxi2, CSBP1, CSBP2, PRKM14, PRKM15, SAPK2A and MAPK14; Han *et al.*, 1993, 1994; Lee *et al.*, 1994), p38β (also known as P38B, SAPK2, p38-2; PRKM11, SAPK2B, P38BETA2 and MAPK11; Jiang *et al.*, 1996), p38γ (also known as ERK3, ERK6, SAPK3, PRKM12, SAPK-3 and MAPK12; Lechner *et al.*, 1996; Li *et al.*, 1996) and p38δ (also known as SAPK4, PRKM13, MGC99536 and MAPK13; Jiang *et al.*, 1997; Kumar *et al.*, 1997). They all share high sequence homology (between 60% and 73% overall) and a canonical dual phosphorylation site T*X*Y in the activation loop (Kyriakis & Avruch, 2001). The tissue distribution, function and activation of the four members of the p38 kinase family have been investigated using a variety of genetic, biological and pharmacological techniques (for reviews of the pathway, see Ono & Han, 2000; Kumar *et al.*, 2003; Zarubin & Han, 2005; Raman *et al.*, 2007). While it is known that p38α plays a significant role in post-transcriptional regulation of cytokine production and inflammatory responses, the normal

roles of the other family members are unknown. Of the four isoforms, p38α and p38β are the most similar, with about 73% sequence identity overall and 95% sequence identity in the ATP-binding site (Fig. 1). Based on analysis of the primary sequence only, it is likely that p38α-selective compounds would also be active against p38β, since selectivity determinants such as Thr106 and Gly110 are conserved between the two enzymes. In fact, the majority of p38 inhibitors reported to date are dual p38α/β inhibitors with almost no activity against the other two isoforms (Hynes & Leftheri, 2005). The dual character of these compounds does not allow their use to differentiate the specific functions and properties of the two enzymes. Although it is not clear whether p38β inhibition could lead to undesirable side effects (*i.e.* p38β knockout mice do not have any known phenotype; Beardmore *et al.*, 2005), some data suggest that a case could be made for the necessity of α-selective over β-selective compounds. For example, recently published data from our laboratories suggested that the inhibition of p38β had no effect on TNF production or regulation of inflammatory response and that specific inhibition of the p38α isoform is necessary and sufficient for anti-inflammatory efficacy *in vivo* (O'Keefe *et al.*, 2007). In addition, the fact that p38α and p38β are differently activated and that they may be differently involved in different biological pathways (Enslen *et al.*, 1998; Somwar *et al.*, 2000; Pramanik *et al.*, 2003; Tourian *et al.*, 2004) suggest that p38β inhibition could be nontherapeutic and possibly unsafe. The first crystal structures of p38α were reported in the late 1990s, both as unliganded enzyme and as a complex with an inhibitor (Wilson *et al.*, 1996, 1997). Since then, several other groups have reported the structure of p38α in complex with a variety of ATP-competitive and non-ATP-competitive inhibitors as well as substrate mimetics. More than 100 different p38α inhibitors have been reported in patents and the literature and a great deal of structural data are available regarding the requirements for p38α inhibition (Lee & Dominguez, 2005). Recently, the structure of p38α in complex with its protein substrate MK2 has also been reported (Haar *et al.*, 2007; White *et al.*, 2007). While the structures of the phosphorylated p38γ isoform (PDB code 1cm8; Bellon *et al.*, 1999) and of the unphosphorylated p38δ isoform (PDB code 3coi; Jiang *et al.*, 1997) have also been reported, there is no structural information to date for the p38β isoform. In order to address some of the p38α *versus* p38β selectivity issues and to aid in the development of p38α-selective compounds, we have determined the three-dimensional structure of human full-length p38β. A double point mutation (C119S,C162S) was indispensable to improve both the homogeneity and crystallizability of the enzyme and to obtain high-resolution data. Here, we report the 2.05 Å resolution structure of the p38β double mutant bound to a nonselective inhibitor. Comparison of this structure with that of the p38α C162S mutant bound to the same inhibitor allows identification of the differences between the two isoforms and points to a path for the design of selective inhibitors.

2. Material and methods

All chromatography columns were purchased from GE Healthcare. The mass of the protein was determined by electrospray mass spectrometry. Dynamic light-scattering (DLS) analysis was carried out using a DynaPro light-scattering instrument (Protein Solutions, now Wyatt Technology); the data were analyzed using their *DYNAMICS* v.2.05 software.

2.1. p38α cloning, expression and crystallization

The cloning, expression, purification and crystallization of the of the C162S mutant of p38α have been described previously (Patel *et al.*, 2004).

2.2. p38β cloning

A full-length cDNA encoding human p38β (UNP code Q15759; Fig. 1) was initially cloned into a pET15b vector. Site-directed mutagenesis was carried out to mutate first residue

```
p38α      GSHMLEMSQERPTFYRQELNKTIWEVPERYQNLSPVGSGAYGSVCAAFDTKTGLRVAVKKLSRPFQ 60
p38β      GSHMLEMSGPRAGFYRQELNKTVWEVPQRLQGLRPVGSGAYGSVCSAYDARLRQKVAVKKLSRPFQ 60
          **  *. *********:****:* *.* ***********:*:*::   :***********

p38α      SIIHAKRTYRELRLLKHMKHENVIGLLDVFTPARSLEEFNDVYLVTHLMGADLNNIVKCQ 120
p38β      SLIHARRTYRELRLLKHLKHENVIGLLDVFTPATSIEDFSEVYLVTTLMGADLNNIVKSQ 120
          *:***:***********:*************** *:*:*.:***** *********** *

p38α      KLTDDHVQFLIYQILRGLKYIHSADIIHRDLKPSNLAVNEDSELKILDFGLARHTDDEMT 180
p38β      ALSDEHVQFLVYQLLRGLKYIHSAGIIHRDLKPSNVAVNEDSELRILDFGLARQADEEMT 180
           *:*:*****:**:**********.**********:********:********::*:***

p38α      GYVATRWYRAPEIMLNWMHYNQTVDIWSVGCIMAELLTGRTLFPGTDHIDQLKLILRLVG 240
p38β      GYVATRWYRAPEIMLNWMHYNQTVDIWSVGCIMAELLQGKALFPGSDYIDQLKRIMEVVG 240
          ************************************ *::****:*:***** *:.:**

p38α      TPGAELLKKISSESARNYIQSLTQMPKMNFANVFIGANPLAVDLLEKMLVLDSDKRITAA 300
p38β      TPSPEVLAKISSEHARTYIQSLPPMPQKDLSSIFRGANPLAIDLLGRMLVLDSDQRVSAA 300
          **..*:* ***** **.*****. **: :::.:* ******:*** :*******:*::**

p38α      QALAHAYFAQYHDPDDEPVADPYDQSFESRDLLIDEWKSLTYDEVISFVPP----PLDQE 356
p38β      EALAHAYFSQYHDPEDEPEAEPYDESVEAKERTLEEWKELTYQEVLSFKPPEPPKPPGSL 360
          :*******:*****:*** *:***:*.*:::  ::***.***:**:** **    * ..

p38α      EMES 360
p38β      EIEQ 364
             *:*.
```

Figure 1
Sequence alignment of p38α (UNP Q16539) and p38β (UNP Q15759) calculated using *ClustalW*2 (Larkin *et al.*, 2007). The two proteins share 73% sequence identity overall and 97% sequence identity in the ATP-binding site (residues highlighted in red). The C162S (in both p38α and p38β) and C119S (in p38β) mutations are highlighted in green. Both enzymes were expressed with an N-terminal His tag (MGSSHHHHHHSSGLVPRGSHMLE) and after removal of the tag by thrombin digestion (see §2) the six residues highlighted in blue were left as part of the final product.

Table 1
Chemical structure, chemical class and IC_{50} for the compounds described in the text.

The wild-type enzymes were used to measure the affinities for the compounds.

Compound	**1** (Fig. 2*a*)	**2** (Fig. 2*b*)	**3** (Fig. 2*c*)	**4** (Fig. 2*d*)
Chemical class	Quinazolinone	Pyridinyl-imidazole	Pyridinyl-imidazole	Pyridinyl-imidazole
IC_{50} (n*M*)				
p38α	0.4	0.08	1.5	26.3
p38β	1.4	0.25	16.4	1175
Ratio β/α	35	3.2	10.9	44.7

162 and then residue 119 from cysteine to serine by QuikChange site-directed mutagenesis (Stratagene). Mutagenesis reactions followed the standard protocol as described by Stratagene. Both mutations were verified by DNA sequencing.

2.3. p38β expression

The same procedure was utilized for the expression of the wild type (WT) and the single and double mutants. *E. coli* BL21 (DE3) competent cells (Novagen) were transformed with the expression vector containing His-tagged p38β using the standard Novagen procedure. The cells were grown at 310 K in Luria–Bertani (LB) medium containing 100 µg ml^{-1} ampicillin to an absorbance of approximately 0.8 at 600 nm. Expression was induced by the addition of 0.1 m*M* isopropyl β-D-1-thiogalactopyranoside (IPTG) after cooling the culture to 289 K. Cells were grown for an additional 16 h at 289 K and then centrifuged at 5500*g* for 15 min. The supernatant was removed and the cell paste was collected for protein purification.

2.4. p38β purification

The cell paste was resuspended in 50 m*M* Tris–HCl pH 7.4, 150 m*M* NaCl, 10% glycerol in the presence of protease inhibitors (Complete EDTA free, Roche Diagnostics) and lysed using a French press at 103 MPa pressure. Lysed cell suspensions were centrifuged at 40 000*g* for 1 h. 500 m*M* NaCl and 20 m*M* imidazole were added to the supernatant before loading it onto a 5 ml HiTrap nickel-chelating column pre-equilibrated with 50 m*M* Tris pH 7.4, 10% glycerol, 1 m*M* TCEP [tris(2-carboxyethyl)phosphine], 500 m*M* NaCl, 20 m*M* imidazole. The column was exhaustively washed with loading buffer followed by buffer containing 40 m*M* imidazole. The protein was then eluted with buffer containing 200 m*M* imidazole. In order to remove any possible spurious phosphorylation, the eluate was incubated at room temperature for 30 min with 1500 U ml^{-1} λ-phosphatase (Calbiochem) in the presence of 2 m*M* Mn^{2+}. The reaction was quenched by adding 5 m*M* EDTA. The His tag was removed by incubating the protein with thrombin [1:1000(*w*:*w*)] at 277 K overnight. The removal of the tag was verified by LC mass spectrometry. 50 m*M* Tris pH 7.4 was added to reduce the salt concentration to approximately 100 m*M*. The resulting solution was loaded onto a pre-equilibrated Resource Q column, from which the protein was eluted with a linear gradient of 0–500 m*M* NaCl in 50 m*M* Tris pH 7.4. The appropriate fractions were then pooled, concentrated, loaded onto a HiLoad 26/60 Superdex 200 column and eluted with 20 m*M* Tris pH 7.4, 100 m*M* NaCl, 5% glycerol and 2 m*M* TCEP. The yield was 3–5 mg l^{-1} with a purity of 99% (as assessed by gel electrophoresis) for the WT and single mutant and 20 mg l^{-1} for the double mutant.

2.5. Kinase assays

Kinase assays were performed as described previously (LoGrasso *et al.*, 1997). The activity of the WT and mutant enzymes was assayed as the final step in the purification procedures. As reported for p38α (Patel *et al.*, 2004), the values obtained for the p38β mutants were within 30% of those measured for the WT enzyme (data not shown).

2.6. Carboxymethylation

Chemical modification of Cys119 was carried out following the reported procedure (Canfield & Anfinsen, 1963); in brief, the reaction was performed following the ion-exchange column by the addition of 10 m*M* iodoacetic acid to 4 mg ml^{-1}

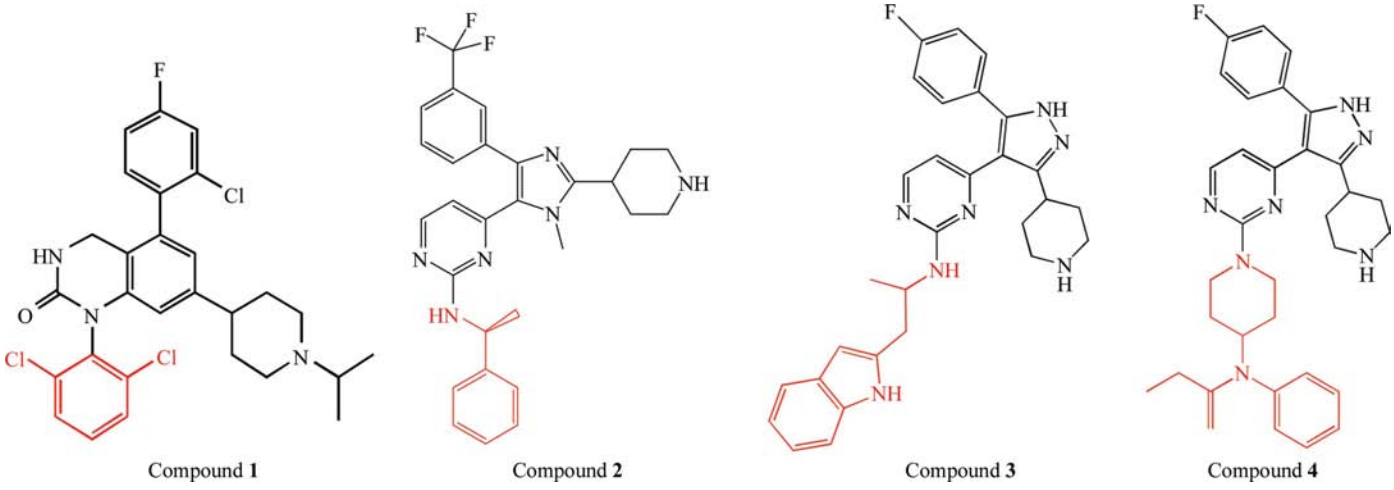

Figure 2
Chemical structures of the compounds described in the text. The portion of the molecule binding in the HP-II is highlighted in red.

Table 2
Data-collection and refinement statistics for the three data sets described in the paper.

Values in parentheses are for the highest resolution bin.

	p38α–compound **1** (3cg7)	p38β(C162S)–compound **1** (3cg8)	p38β(C119S,162S)–compound **1** (3cg9)
Data collection			
Space group	$P2_12_12_1$	$P2_1$	$P2_1$
Unit-cell parameters (Å, °)	a = 44.9, b = 88.0, c = 121.8, $\alpha = \beta = \gamma$ = 90.0	a = 39.1, b = 157.7, c = 60.4, $\alpha = \gamma$ = 90.0, β = 91.6	a = 39.2, b = 158.8, c = 60.9, $\alpha = \gamma$ = 90.0, β = 91.6
Resolution (Å)	50.0–1.8 (1.86–1.8)	30.0–2.4 (2.5–2.4)	50.–2.05 (2.12–2.05)
No. of reflections	44651 (4350)	28642 (2712)	45759 (4216)
Completeness (%)	98.7 (97.6)	99.2 (94.0)	98.5 (92.0)
Redundancy	7.1 (6.9)	4.9 (4.7)	5.3 (3.5)
$\langle I/\sigma(I)\rangle$	15.8 (4.1)	8.9 (1.2)	8.8 (1.6)
$R_{\rm merge}$†	6.1 (26.0)	8.8 (33.6)	5.8 (26.3)
Refinement			
Resolution (Å)	30.0–1.8 (1.85–1.8)	30.0–2.4 (2.57–2.4)	30.0–2.05 (2.16–2.05)
No. of reflections	44589 (3115)	28486 (5138)	45713 (6276)
Completeness (%)	98.5 (95.2)	99.8 (99.9)	98.5 (93.4)
$R_{\rm free}/R$ factor	20.8/18.2 (25.9/20.7)	27.2/20.8 (31.0/22.9)	27.5/22.2 (33.4/25.0)
R.m.s.d. bond length (Å)	0.010	0.012	0.011
R.m.s.d. bond angle (°)	1.230	1.389	1.315
Ramachandran‡	89.9/9.2/0.9/0.0	86.4/11.9/1.7/0.0	87.1/11.9/1.0/0.0
$\langle B\rangle$ (Å^2)	20.9	35.0	33.4
No. of protein atoms/ molecules in ASU	2848/1	5388/2	5388/2
No. of solvent atoms	453	152	344
No. of ligand atoms	36	72	72
No. of ions	0	3	3

† R linear as defined in *HKL*-2000 (Otwinowski & Minor, 1997): $\sum(|I - \langle I\rangle|)/\sum(I)$. ‡ Percentage of residues in the allowed, additionally allowed, generously allowed and disallowed regions of the Ramachandran plot (Laskowski *et al.*, 1993).

p38β in 50 m*M* Tris pH 7.4, 75 m*M* NaCl. The reaction was allowed to proceed for 20 min at room temperature. The entire sample was immediately run on a Superdex 200 column to remove the reactants and then treated exactly as the unmodified sample. Mass spectrometry indicated a mass that was consistent with the quantitative modification of one cysteine.

2.7. p38β crystallization

The protein fractions from the Superdex 200 column were directly concentrated to 10 mg ml^{-1} by centrifugal ultrafiltration and incubated with a twofold molar excess of compound **1** (Table 1, Fig. 2) in 20 m*M* Tris pH 7.4, 100 m*M* NaCl, 5% glycerol and 2 m*M* TCEP. DLS analysis was routinely performed on all p38β samples prior to setting up crystallization trials. Small crystals of the single mutant after carboxymethylation were initially obtained using vapor diffusion in hanging drops: 1 µl protein solution and 1 µl reservoir solution (12–14% PEG 3350, 0.12 *M* ammonium fluoride) were mixed and the drop was allowed to equilibrate against 0.5 ml reservoir solution. Detergent screening led to the identification of CTAB (cetyl trimethylammonium bromide; Hampton Research) as a useful additive and sizable crystals were obtained in hanging drops by mixing 1 µl protein solution (10 mg ml^{-1} in 20 m*M* Tris pH 7.4, 100 m*M* NaCl, 5% glycerol, 2 m*M* TCEP) and 1 µl reservoir solution (12% PEG 3350, 0.12 *M* ammonium fluoride, 30 µ*M* CTAB) and equilibrating against 0.5 ml reservoir solution. These crystals diffracted to about 2.4 Å resolution using synchrotron radiation (see below) and were used to solve the structure of p38β. Crystals of the double C119S,C162S mutant were obtained after pre-incubation of the protein (10 mg ml^{-1} in 20 m*M* Tris pH 7.4, 100 m*M* NaCl, 5% glycerol and 2 m*M* TCEP) with a twofold molar excess of compound **1** and 500 m*M* $ZnCl_2$ for about 2 h in ice; crystals were obtained in hanging drops by mixing 1 µl protein solution and 1 µl reservoir solution and equilibrating against 0.5 ml of a reservoir solution containing 12–14% PEG, 0.12 *M* ammonium fluoride, 1% DMSO, 30 µ*M* CTAB and 10–20 m*M* LiCl. These crystals diffracted to better than 2.1 Å resolution.

2.8. Data collection and structure solution and refinement

Data for the p38α–compound **1** complex were collected using synchrotron radiation from a single crystal flash-frozen at 100 K. Before freezing, the crystal was cryoprotected by 15 min soaks in 5%, 10% and 15% glycerol in reservoir solution. Data were collected using a wavelength of 1 Å on beamline 17ID in the facilities of the Industrial Macromolecular Crystallographic Association (IMCA) at the Advanced Photon Source, Argonne, Illinois, USA. The data were processed with *HKL*-2000 (Otwinowski & Minor, 1997). The crystals were isomorphous with the previously reported crystals of p38α. The bound ligand was identified in difference Fourier electron-density maps using PDB entry 1r3c (Patel *et al.*, 2004) as a starting model. Refinement was carried out for the first five cycles with *CNX* (Brünger *et al.*, 1998; Accelrys) and for the last four cycles with *REFMAC* (Murshudov *et al.*, 1997, 1999; Pannu *et al.*, 1998) as implemented in the *CCP*4 package (Collaborative Computational Project, Number 4, 1994). The refinement libraries for the ligand were generated using the standard scripts supplied by *CNX* (*XPLOR*2*D*) and *CCP*4. Manual rebuilding of the model was performed in *O* (Kleywegt *et al.*, 2001*a*,*b*; Jones & Kjeldgaard, 1997). Final validation of the model was carried out using *PROCHECK* (Laskowski *et al.*, 1993). Statistics for data collection and structure refinement are reported in Table 2. The coordinates of the complex of p38α with compound **1** have been deposited with the PDB (accession code 3gc7).

Data for both the single and the double mutants of p38β in complex with compound **1** were collected using synchrotron radiation from single crystals flash-frozen at 100 K. Before freezing, the crystals were cryoprotected by quickly placing them into three solutions containing increasing amounts (6%,

12% and 15%) of glycerol in reservoir solution. Data were collected on beamlines 17ID (single mutant) and 17BM (double mutant) at IMCA. Data were processed with *HKL*-2000 (Otwinowski & Minor, 1997). The structure of the single mutant was solved by molecular replacement using *MOLREP* (Vagin & Teplyakov, 1997) as implemented in the *CCP*4 package (Collaborative Computational Project, Number 4, 1994) with the structure of the p38α–compound **1** complex (without waters or bound ligand) as the search model. The structure was refined with *CNX* (Brünger *et al.*, 1998; Accelrys), *autoBUSTER* (Vonrhein & Bricogne, 2003; Bricogne *et al.*, 2008) and *REFMAC* (Murshudov *et al.*, 1997, 1999; Pannu *et al.*, 1998); extensive manual rebuilding of the model was required during refinement and was performed in *O* (Kleywegt *et al.*, 2001*a*,*b*; Jones & Kjeldgaard, 1997). Simulated-annealing OMIT maps were used throughout the refinement to validate the model. Electron density for the bound ligand was evident from the very beginning of the refinement, but the ligand was only modeled after all possible protein density had been assigned. Three cation-binding sites, two at the crystallographic interface and one at the noncrystallographic interface, were also identified during the refinement. Based on the atom type, residue type and distance of the protein atoms surrounding the sites (analyzed using the tables reported at http://tanna.bch.ed.ac.uk/) the two cations at the crystallographic interface were modeled as sodium ions, while that at the noncrystallographic interface, which was clearly heavier than sodium, was modeled as nickel. The values of the temperature factors obtained for these ions at the end of the refinement (comparable to those of the surrounding atoms) confirmed that the assignment was correct. The refined structure of the single mutant was then used as a starting point for refinement of the double mutant. The resolution was slowly increased from 2.4 to 2.05 Å, alternating cycles of manual inspection and rebuilding of the model and computer-based refinement [*CNX* (Brünger *et al.*, 1998; Accelrys), *autoBUSTER* (Vonrhein & Bricogne, 2003; Bricogne *et al.*, 2008) and *REFMAC* (Murshudov *et al.*, 1997, 1999; Pannu *et al.*, 1998)]. The loop containing the second mutation (residues Asp114–Glu125) was removed from the starting model and rebuilt into available density. Final analysis of the model was carried out with *PROCHECK* (Laskowski *et al.*, 1993). Statistics for data collection and structure refinement are reported in Table 2. The coordinates for both structures have been deposited with the PDB (accession codes 3gc8 and 3gc9, respectively).

3. Results and discussion

3.1. Structure of the p38α–compound 1 complex

The properties of quinazolinone compounds such as **1** (Table 1, Fig. 2) and the structural basis for their potency and selectivity have been extensively described (Stelmach *et al.*, 2003; Fitzgerald *et al.*, 2003). In brief, compound **1** binds to the ATP-binding pocket of p38α (Fig. 3*a*); its dihydroquinazolinone core makes three hydrogen-bond interactions with the main-chain atoms of residues of the linker region, specifically the main-chain O atom of His107 and the main-chain N atoms of Met109 and Gly110. This last interaction is the consequence of a ligand-induced peptide flip between Met109 and Gly110; this peptide flip is characteristic of dihydroquinazolinones and related compounds and is one of the determinants of the high p38α and p38β selectivity (Fitzgerald *et al.*, 2003) observed for these compounds. The remaining interactions between the compound and the protein are mostly hydrophobic in nature. The piperidine ring extends under the Gly-rich loop (Val30–Ser40) and is stacked in a side-to-face fashion with the side chain of Tyr35. The dichlorophenyl ring occupies the hydrophobic pocket (HP-I) at the back of the ATP-binding site (Scapin, 2002). It has now been known for over a decade that highly selective p38α and p38β compounds utilize this pocket. In p38α and p38β the gatekeeper residue is a relatively small threonine (Thr106) that allows the binding of large substituents, but the larger methionine or glutamine residues that are present in all other MAP kinases prevent the binding of such compounds (Gum *et al.*, 1998; Wilson *et al.*, 1997; Eyers *et al.*, 1998; Lisnock *et al.*, 1998). The third substituent of the dihydroquinazolinone core (the chlorofluorophenyl ring) extends through the so-called hydrophobic pocket 2 (HP-II; Scapin, 2002) into the solvent. Given the high primary sequence similarity between p38α and p38β (Fig. 1), the three-dimensional structure of the p38β isoform was sought to help in addressing selectivity issues.

3.2. Crystallization of p38β

Attempts to obtain diffraction-quality crystals using the WT enzyme were unsuccessful. Our previous work on p38α had shown that the mutation of Cys162 to serine helped to stabilize the enzyme, reducing the aggregation problems observed upon storage (Patel *et al.*, 2004). The same approach was applied to p38β and the single mutant (C162S) was generated. This mutant produced small preliminary crystals, which were of poor quality and difficult to reproduce. Both p38α and p38β have a second exposed cysteine (Cys119 in both enzymes) and although this residue did not prevent the crystallization of p38α, we investigated the possibility that modification of this second cysteine could be beneficial in the crystallization of p38β. p38β was carboxymethylated and the modified protein produced diffraction-quality crystals under the same conditions as initially identified for the unmodified enzyme. Data collected from these chemically modified crystals were used to solve the initial structure of p38β. Subsequently, since modification of Cys119 seemed to be necessary to further stabilize the protein and obtain reproducible crystals, the double mutant C119S,C162S was constructed and structural work was pursued using this construct. In addition, the initial crystal structure of the single mutant, with two molecules per asymmetric unit, showed the presence of three cation-binding sites: two at the crystallographic interface and one at the noncrystallographic interface. This ion was modeled as Ni^{2+}. The Ni^{2+} ion probably leached from the Ni–NTA column used during purification: this finding, together with the fact that DLS

experiments indicated that the protein sample that crystallized had a molecular weight corresponding to a dimer, suggested that the controlled inclusion of cations in the protein buffers could induce the formation of the dimeric form that was found in the crystals. Usage of 10–20 m*M* cations tremendously improved the quality and size of the crystals and allowed a 2.05 Å resolution data set to be collected.

3.3. Structure of the p38β–compound 1 complex

Although the structure of p38β was initially solved using 2.4 Å resolution X-ray diffraction data collected from the C162S mutant carboxymethylated at Cys119, once higher resolution data became available for the double mutant refinement was completed against this second data set. The structures of the single and double mutant are very similar (the r.m.s.d. for main-chain atoms is 0.177 Å) and all the following descriptions and comparisons were performed using the coordinates of the double mutant. The 2.05 Å structure of p38β contains residues 3–172 and 184–348 for the first monomer and residues 2–173 and 183–349 for the second monomer. No electron density was visible for the activation loop (residues 173–183) in either monomer. The two monomers in the asymmetric unit are substantially identical (the r.m.s.d. on C^{α} atoms for 325 residues is 0.725 Å), with the exception of the loop spanning residues 242–266, which

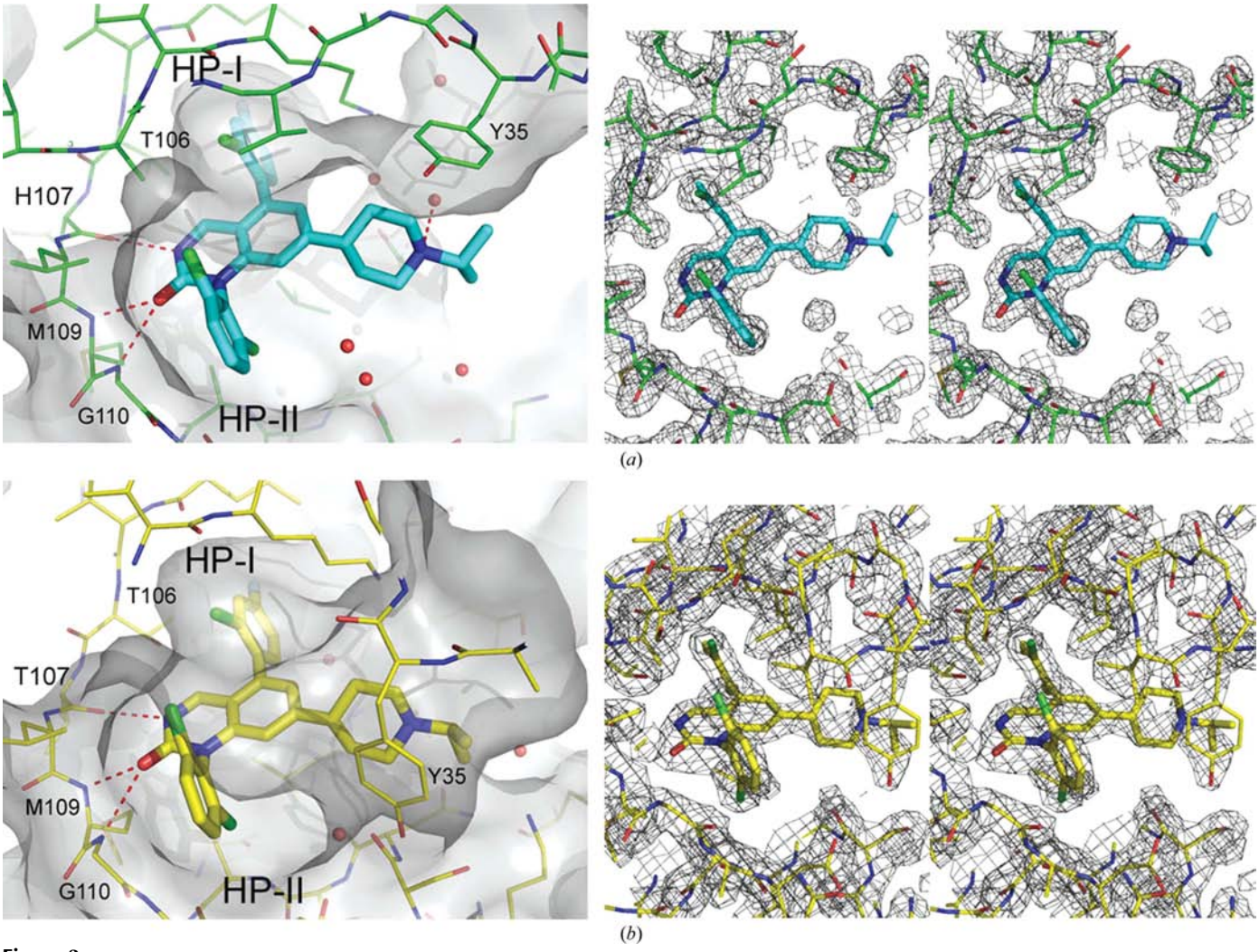

Figure 3
(*a*) Left panel: compound **1** bound to p38α: compound **1** is shown as sticks and p38 as thick lines. Hydrogen-bond interactions are shown as dotted red lines. The molecular surface of the protein is represented in gray. Compound **1** binds in the ATP-binding site, where it interacts with residues of the linker region (His107–Gly110) and of the glycine-rich loop (Tyr35). It occupies hydrophobic pocket 1 (HP-I) and extends through hydrophobic pocket 2 (HP-II) into the outside solvent area. This and all other figures were produced using *PyMOL* (DeLano Scientific). Right panel: stereoview of the electron density ($2F_o - F_c$ map calculated without the bound ligand and contoured at 1.2σ) for the same region of the binding site; the orientation of the two panels is the same and labels have been omitted from the right panel for clarity. (*b*) Left panel: compound **1** bound to p38β: compound **1** is shown as sticks and p38 as thick lines. Hydrogen-bond interactions are shown as dotted red lines. The molecular surface of the protein is represented in gray. Compound **1** binds in the ATP-binding site, where it interacts with residues of the linker region (Thr107–Gly110) and of the glycine-rich loop (Tyr35). As observed for p38α, it occupies hydrophobic pocket 1 (HP-I) and extends through hydrophobic pocket 2 (HP-II) into the solvent-exposed area. Right panel: stereoview of the electron density ($2F_o - F_c$ map calculated without the bound ligand and contoured at 1.2σ) for the same region of the binding site; the orientation of the two panels is the same and labels have been omitted from the right panel for clarity.

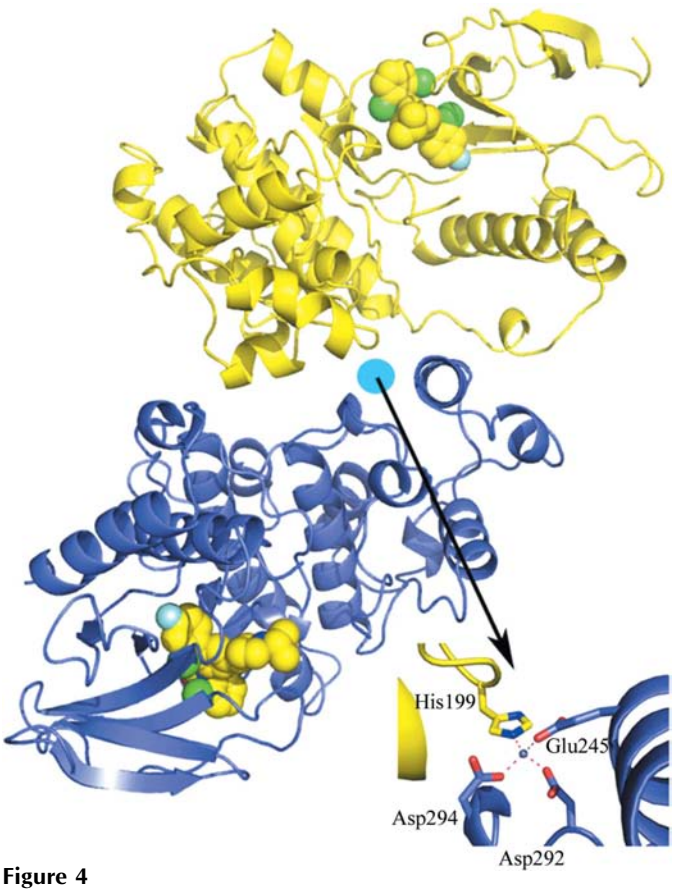

Figure 4
The p38β dimer: the bound compound **1** is shown as yellow spheres. The inset shows the interactions made by the Zn ion with protein residues (yellow and blue C atoms identify the two molecules in the asymmetric unit).

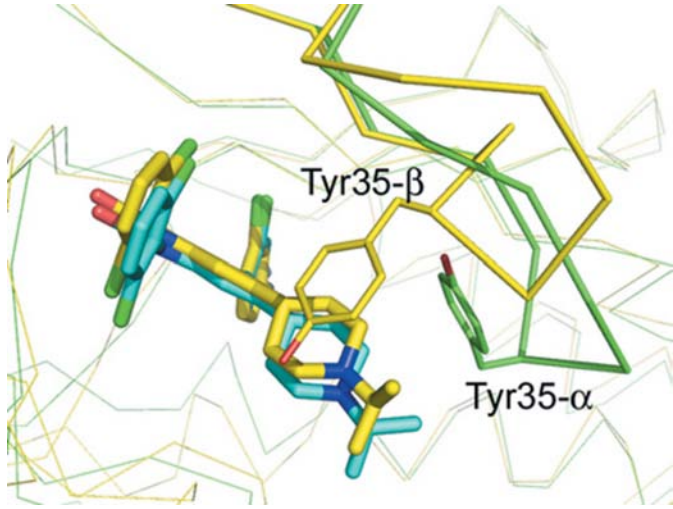

Figure 5
Comparison between the conformation of the glycine-rich loop in p38α (green trace) and p38β (yellow trace). The interaction of the side chain of Tyr35 with the bound ligand is also different in the two isoforms: in p38β it stacks with the piperidine ring in a face-to-face fashion, while in p38α the orientation is more side-to-face.

appears to be more disordered in one of the monomers than in the other. The following description is therefore based on one of the monomers (referred to as monomer *A*) and differences will be pointed out if necessary.

The overall fold of p38β resembles that of a typical kinase, with a smaller mostly β-sheet N-terminal domain and a larger mostly α-helical C-terminal domain (Scapin, 2002). The two domains are linked by a single polypeptide chain (the linker region; residues Thr107–Gly110). The ATP-binding site, which is the target site for most kinase inhibitors to date, is located between the two domains. p38β crystallized with a dimer in the asymmetric unit (Fig. 4) and although the physiological entity is monomeric, DLS experiments showed that the preferred quaternary form under crystallization conditions is a dimer (data not shown). The dimerization was induced by divalent cations (Ni^{2+} or Zn^{2+}) either derived from the purification steps or added in a controlled fashion. The ion mediates the assembly of the two monomers by interacting with His199 of one monomer and Glu245, Asp292 and Asp294 of the other (Fig. 4).

Compound **1** binds to the ATP-binding site and, not surprisingly, makes the same interactions observed in the p38α–compound **1** complex (Fig. 3*b*). It forms the same three hydrogen-bond interactions with the main-chain atoms of the linker region residues, including that with the main-chain N atom of Gly110: this last interaction is probably the consequence of a compound-induced peptide flip (between Met109 and Gly110), as observed in p38α, and has been shown to be one of the determinants of the high p38α and p38β selectivity observed for the dihydroquinazolinones and related compounds (Fitzgerald *et al.*, 2003). The most interesting difference is that the position of the tip of the Gly-rich loop (Gly31–Ser37) is different in p38β from that in p38α (Fig. 5); while in p38α residues 31–37 assume an extended conformation [two β-strands linked by a type III β-turn (Richardson, 1981) at Ala34–Tyr35], in p38β residues 33–38 assume a helical conformation (based on their φ, ψ angles). The interaction of the side chain of Tyr35 with the bound ligand is also different in the two isoforms: in p38β it stacks with the piperidine ring in a face-to-face fashion, while in p38α the orientation is more side-to-face. The most striking consequence of this different conformation is that the portion of the ATP-binding site occupied by the piperidine in p38β is more shielded from the solvent than in p38α. Nevertheless, this may be seen as being caused by the intrinsically high flexibility of the Gly-rich loop rather than as a characteristic of p38β, since a similar conformation of the Gly-rich loop has been found in other complexes of p38α (Natarajan *et al.*, 2006; Fitzgerald *et al.*, 2003).

3.4. Structural comparison between the two isoforms

Both crystal structures have been solved in their inactive state (*i.e.* no phosphorylation on the activation loop) and more pronounced differences might arise between the two isoforms upon activation. Nevertheless, since most p38 inhibitors bind to the inactive form of the kinase, structural information derived from the inactive conformations can still be used to define some, if not all, of the selectivity determinants between

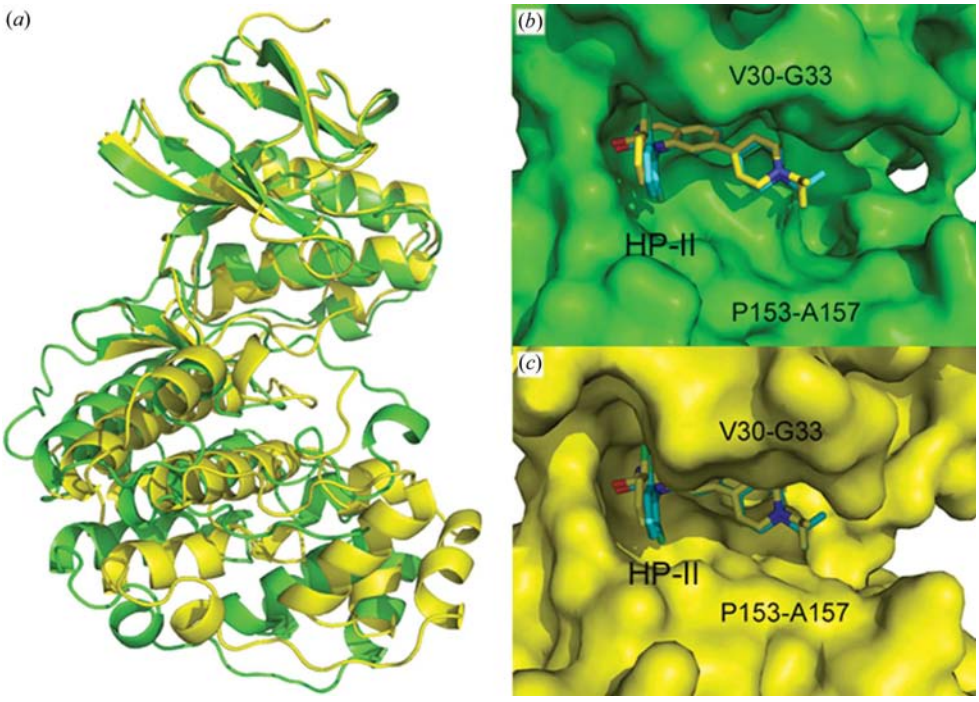

Figure 6
Comparison between the three-dimensional structures of p38α C162S (protein colored green and ligand colored cyan) and p38β C119S,C162S (protein and ligand colored yellow). (*a*) Overlay of the C$^{\alpha}$ traces. The overlay was performed by aligning the two N-terminal domains. (*b*, *c*) Surface representation of the ATP-binding site as viewed through hydrophobic pocket 2 in p38α (green) and p38β (yellow). To provide a clearer view of the binding site, the side chain of Tyr35 was omitted in the surface calculation. It is clear that the different orientation of the two domains causes hydrophobic pocket 2 in p38β to be smaller than in p38α.

the two isoforms. Fig. 6(*a*) shows an overlay of the C$^{\alpha}$ traces of p38β (yellow) and p38α (green). The two individual domains in the two isoforms are very similar: the r.m.s.d.s on C$^{\alpha}$ atoms for the N-terminal and C-terminal domains are 0.73 and 1.07 Å, respectively. On the other hand, the relative orientation of the N- and C-terminal domains in the two isoforms is different. The overlay on which the following discussion is based was performed using the N-terminal domain, since the ligand mostly interacts with this domain. In this overlay the C-terminal domain of p38β is rotated inward (towards a more closed conformation compared with p38α) by approximately 30°. While the residues lining the binding site are virtually identical, the different domain rotation causes an approximately 2 Å reduction in the width of HP-II (Figs. 6*b* and 6*c*). Even without considering the difference in conformation and position of the flexible Gly-rich loop, it is clear that the C-terminal domain (identified in Fig. 6 by the polypeptide spanning residues Pro153–Ala157) has moved closer to the N-terminal domain (identified in Fig. 6 by residues Val30–Gly33): the size of the opening (as measured from the main chain of residues Pro153–Ala157 to the main chain of residues Val30–Gly33) in p38α is 14.8 Å and is reduced to 12.9 Å in p38β. Many of the reported p38 inhibitors bind with some groups located in HP-II and this analysis suggested that modulating the size, length and flexibility of the substituent in this pocket could lead to selectivity. With this idea, we revisited some compounds belonging to an older structural class (pyridinyl-imidazole compounds; Table 1, Fig. 2; compounds **2**–**4**). The structure and properties of this class of compounds have been extensively reported (Wilson *et al.*, 1997; Liverton *et al.*, 1999; Fitzgerald *et al.*, 2003). The binding mode of compound **2** is known (Fitzgerald *et al.*, 2003) and shows that the aminopyrimidine is located within the HP-II; compounds **3** and **4** were selected because they are characterized by the presence of larger and more rigid substituents in the region corresponding to HP-II binding. These compounds were assayed in the standard kinase assay (LoGrasso *et al.*, 1997) and clearly showed a decrease in affinity towards p38β (Table 1); this effect is more pronounced in the case of compound **4**, probably because the *N*-(2-)1*H*-indol-2-yl)-1-methylethyl]-pyrimidin-2-amine of compound **3** is much more flexible and thus easier to accommodate than the (1-methylenepropyl)-*N*-phenyl-piperidin-4-amine of compound **4**. This result clearly lends significant experimental support to our hypothesis. As reported for similar cases (Scapin *et al.*, 2003; Asante-Appiah *et al.*, 2006), targeting conformational changes with the help of structural knowledge may represent a viable path to differentiate between very closely related members of the same family.

4. Conclusions

We report here the crystal structure of the p38β isoform, solved and refined to 2.05 Å resolution. Mutation of Cys162 to serine and subsequent modification of Cys119, either by carboxymethylation or mutation to serine, played a critical role in obtaining diffraction-quality crystals. Although p38β is homologous to p38α in both primary sequence and tertiary structure, knowledge of the three-dimensional structure allowed the identification of conformational differences in the ATP-binding site that may be utilized for the design of p38α-selective compounds.

Use of the IMCA-CAT beamline 17-ID and 17-BM at the Advanced Photon Source was supported by the companies of the Industrial Macromolecular Crystallography Association

through a contract with the Center for Advanced Radiation Sources at the University of Chicago.

References

Asante-Appiah, E., Patel, S., Desponts, C., Taylor, J. M., Lau, C., Dufresne, C., Therien, M., Friesen, R., Becker, J. W., Leblanc, Y., Kennedy, B. P. & Scapin, G. (2006). *J. Biol. Chem.* **281**, 8010–8015.

Beardmore, V. A., Hinton, H. J., Eftychi, C., Apostolaki, M., Armaka, M., Darragh, J., McIlrath, J., Carr, J. M., Armit, L. J., Clacher, C., Malone, L., Kollias, G. & Arthur, J. S. C. (2005). *Mol. Cell. Biol.* **25**, 10454–10464.

Bellon, S., Fitzgibbon, M. J., Fox, T., Hsiao, H. M. & Wilson, K. P. (1999). *Structure*, **7**, 1057–1065.

Bricogne, G., Blanc, E., Brandl, M., Flensburg, C., Keller, P., Paciorek, W., Roversi, P., Smart, O. S., Vonrhein, C. & Womack, T. (2008). *BUSTER-TNT* 2.5.1 and *autoBUSTER* 1.3.1. Cambridge: Global Phasing Ltd.

Brünger, A. T., Adams, P. D., Clore, G. M., DeLano, W. L., Gros, P., Grosse-Kunstleve, R. W., Jiang, J.-S., Kuszewski, J., Nilges, M., Pannu, N. S., Read, R. J., Rice, L. M., Simonson, T. & Warren, G. L. (1998). *Acta Cryst.* D**54**, 905–921.

Canfield, R. E. & Anfinsen, C. B. (1963). *J. Biol. Chem.* **238**, 2684–2690.

Collaborative Computational Project, Number 4 (1994). *Acta Cryst.* D**50**, 760–763.

Enslen, H., Raingeaud, J. & Davis, R. J. (1998). *J. Biol. Chem.* **273**, 1741–1748.

Eyers, P. A., Craxton, M., Morrice, N., Cohen, P. & Goedert, M. (1998). *Chem. Biol.* **5**, 321–328.

Fitzgerald, C. E., Patel, S. B., Becker, J. W., Cameron, P. M., Zaller, D., Pikounis, V. B., O'Keefe, S. J. & Scapin, G. (2003). *Nature Struct. Biol.* **10**, 764–769.

Gum, R. J., McLaughlin, M. M., Kumar, S., Wang, Z., Bower, M. J., Lee, J. C., Adams, J. L., Livi, G. P., Goldsmith, E. J. & Young, P. R. (1998). *J. Biol. Chem.* **273**, 15605–15610.

Haar, E. ter, Prabakhar, P., Liu, X. & Lepre, C. (2007). *J. Biol. Chem.* **282**, 9733–9739.

Han, J., Lee, J. D., Bibbs, L. & Ulevitch, R. J. (1994). *Science*, **265**, 808–811.

Han, J., Lee, J. D., Tobias, P. S. & Ulevitch, R. J. (1993). *J. Biol. Chem.* **268**, 25009–25014.

Hynes, J. & Leftheri, K. (2005). *Curr. Top. Med. Chem.* **5**, 967–985.

Jiang, Y., Chen, C., Li, Z., Guo, W., Gegner, J. A., Lin, S. & Han, J. (1996). *J. Biol. Chem.* **271**, 17920–17926.

Jiang, Y., Gram, H., Zhao, M., New, L., Gu, J., Feng, L., Di Padova, F., Ulevitch, R. J. & Han, J. (1997). *J. Biol. Chem.* **272**, 30122–30128.

Jones, A. T. & Kjeldgaard, M. (1997). *Methods Enzymol.* **277**, 173–208.

Kleywegt, G. J., Zou, J.-Y., Kjeldgaard, M. & Jones, T. A. (2001*a*). *International Tables for Crystallography*, Vol. *F*, edited by M. G. Rossmann & E. Arnold, pp. 353–356. Dordrecht: Kluwer Academic Publishers.

Kleywegt, G. J., Zou, J.-Y., Kjeldgaard, M. & Jones, T. A. (2001*b*). *International Tables for Crystallography*, Vol. *F*, edited by M. G. Rossmann & E. Arnold, pp. 366–367. Dordrecht: Kluwer Academic Publishers.

Kumar, S., Boehm, J. & Lee, J. C. (2003). *Nature Rev. Drug. Discov.* **2**, 717–726.

Kumar, S., McDonnell, P. C., Gum, R. J., Hand, A. T., Lee, J. C. & Young, P. R. (1997). *Biochem. Biophys. Res. Commun.* **235**, 533–538.

Kyriakis, J. M. & Avruch, J. (2001). *Physiol. Rev.* **81**, 807–869.

Larkin, M. A., Blackshields, G., Brown, N. P., Chenna, R., McGettigan, P. A., McWilliam, H., Valentin, F., Wallace, I. M., Wilm, A., Lopez, R., Thompson, J. D., Gibson, T. J. & Higgins, D. G. (2007). *Bioinformatics*, **23**, 2947–2948.

Laskowski, R. A., MacArthur, M. W., Moss, D. S. & Thornton, J. M. (1993). *J. Appl. Cryst.* **26**, 283–291.

Lechner, C., Zahalka, M. A., Giot, J. F., Moller, N. P. & Ullrich, A. (1996). *Proc. Natl Acad. Sci. USA*, **93**, 4355–4359.

Lee, J. C., Laydon, J. T., McDonnell, P. C., Gallagher, T. F., Kumar, S., Green, D., McNulty, D., Blumenthal, M. J., Heys, J. R. & Landvatter, S. W. (1994). *Nature (London)*, **372**, 739–746.

Lee, M. R. & Dominguez, C. (2005). *Curr. Med. Chem.* **12**, 2979–2994.

Li, Z., Jiang, Y., Ulevitch, R. J. & Han, J. (1996). *Biochem. Biophys. Res. Commun.* **228**, 334–340.

Lisnock, J., Tebben, A., Frantz, B., O'Neill, E. A., Croft, G., O'Keefe, S. J., Li, B., Hacker, C., de Laszlo, S., Smith, A., Libby, B., Liverton, N., Hermes, J. & LoGrasso, P. (1998). *Biochemistry*, **37**, 16573–16581.

Liverton, N. J. *et al.* (1999). *J. Med. Chem.* **42**, 2180–2190.

LoGrasso, P. V., Frantz, B., Rolando, A. M., O'Keefe, S. J., Hermes, J. D. & O'Neill, E. A. (1997). *Biochemistry*, **36**, 10422–10427.

Murshudov, G. N., Vagin, A. A. & Dodson, E. J. (1997). *Acta Cryst.* D**53**, 240–255.

Murshudov, G. N., Vagin, A. A., Lebedev, A., Wilson, K. S. & Dodson, E. J. (1999). *Acta Cryst.* D**55**, 247–255.

Natarajan, S. R., Heller, S. T., Nam, K., Singh, S. B., Scapin, G., Patel, S., Thompson, J. E., Fitzgerald, C. E. & O'Keefe, S. J. (2006). *Bioorg. Med. Chem. Lett.* **16**, 5809–5813.

O'Keefe, S. J., Mudgett, J. S., Cupo, S., Parsons, J. N., Chartrain, N. A., Fitzgerald, C., Chen, S.-L., Lowitz, K., Rasa, C., Visco, D., Luell, S., Carballo-Jane, E., Owens, K. & Zaller, D. M. (2007). *J. Biol. Chem.* **282**, 34663–34671.

Ono, K. & Han, J. (2000). *Cell. Signal.* **12**, 1–13.

Otwinowski, Z. & Minor, W. (1997). *Methods Enzymol.* **276**, 307–326.

Pannu, N. S., Murshudov, G. N., Dodson, E. J. & Read, R. J. (1998). *Acta Cryst.* D**54**, 1285–1294.

Patel, S. B., Cameron, P. M., Frantz-Wattley, B., O'Neill, E., Becker, J. W. & Scapin, G. (2004). *Biochim. Biophys. Acta*, **1696**, 67–73.

Pramanik, R., Qi, X., Borowicz, S., Choubey, D., Schultz, R. M., Han, J. & Chen, G. (2003). *J. Biol. Chem.* **278**, 4831–4839.

Raman, M., Chen, W. & Cobb, M. H. (2007). *Oncogene*, **26**, 3100–3112.

Richardson, J. S. (1981). *Adv. Protein Chem.* **34**, 167–339.

Scapin, G. (2002). *Drug Discov. Today*, **7**, 601–611.

Scapin, G. *et al.* (2003). *Biochemistry*, **42**, 11451–11459.

Somwar, R., Perreault, M., Kapur, S., Taha, C., Sweeney, G., Ramlal, T., Kim, D. Y., Keen, J., Cote, C. H., Klip, A. & Marette, A. (2000). *Diabetes*, **49**, 1794–1800.

Stelmach, J. E. *et al.* (2003). *Bioorg. Med. Chem. Lett.* **13**, 277–280.

Tourian, L., Zhao, H. & Srikant, C. B. (2004). *J. Cell Sci.* **117**, 6459–6471.

Vagin, A. & Teplyakov, A. (1997). *J. Appl. Cryst.* **30**, 1022–1025.

Vonrhein, C. & Bricogne, G. (2003). *autoBUSTER* version 0.0.7. *An Automated System for Macromolecular Refinement Using BUSTER-TNT.* Cambridge: Global Phasing Ltd.

White, A., Pargellis, C. A., Studts, J. M., Werneburg, B. G. & Farmer, B. T. (2007). *Proc. Natl Acad. Sci. USA*, **104**, 6353–6358.

Wilson, K. P., Fitzgibbon, M. J., Caron, P. R., Griffith, J. P., Chen, W., McCaffrey, P. G., Chambers, S. P. & Su, M. S. S. (1996). *J. Biol. Chem.* **271**, 27696–27700.

Wilson, K. P., McCaffrey, P. G., Hsiao, K., Pazhanisamy, S., Galullo, V., Bemis, G. W., Fitzgibbon, M. J., Caron, P. R., Murcko, M. A. & Su, M. S. (1997). *Chem. Biol.* **4**, 423–431.

Zarubin, T. & Han, J. (2005). *Cell Res.* **15**, 11–18.